Arch. Metall. Mater. **68** (2023), 1, 339-344

DOI: https://doi.org/10.24425/amm.2023.141510

A. NALBORCZYK-KAZANECKA[1,2*], G. MROWKA-NOWOTNIK[1]

THE EFFECT OF THE PARAMETERS OF ROBOTIC TIG WELDING ON THE MICROSTRUCTURE OF 17-4PH STAINLESS STEEL WELDED JOINT

17-4PH stainless steel finds application in the aerospace industry owing to its good mechanical properties and corrosion resistance. In the literature, this steel is described as good for welding, but research shows that it may be problematic due to the formation of defects. In this study, the welded joints were made by the robotic TIG welding method with various welding speeds (2 and 3 mm/s). The joints were subjected to non-destructive testing and were free from defects. The microstructure was observed by light microscopy and scanning electron microscopy. Changes in the microstructure of the heat affected zone were observed and discussed. Based on the observation of the microstructure and the change in the hardness profile, the heat affected zone was divided into 4 characteristic regions. δ-ferrite and NbC were observed in the martensite matrix. The welded joints were subjected to heat treatment consisting of solution and aging in 550°C for 4 h. The microstructure of the heat affected zone become homogenized as a result of the heat treatment. The content of stable austenite in the welded joint after the heat treatment was about 3%.

Keywords: welding; 17-4PH stainless steel; precipitation hardening; heat treatment

1. Introduction

The precipitation hardening steels are a family of corrosion resistance alloys some of which have high strength and weight ratio making them ideal materials for a range of uses. Thus, they find various application in the industry, e.g. in the aerospace, nuclear and marine industries. In order to obtain the precipitation reaction, alloying elements such as aluminium, titanium, copper or molybdenum are added either without highlighting or in combination. The corrosion resistance is achieved by the addition of chromium. The addition of chromium causes the formation of protective chromium oxide [1-3]. There are three basic classes of precipitation hardening (PH) steels: martensitic PH stainless steels, austenitic PH stainless steels and semi-austenitic PH stainless steels [1,4,5]

17-4PH SS is a martensitic precipitation hardening stainless steel. Corrosion resistance is better than in case of regular martensitic stainless steel [1]. Owing to the combination of high mechanical properties and good corrosion resistance, 17-4PH SS is used in aircraft components, pressure vessels, impellers [6,9-11]. This class of steels has martensite finish temperature (M_f) just above the room temperature. For the 17-4PH SS, the M_s (martensite start) – M_f (martensite finish) temperature ranges from 130 to 30°C [1]. While cooling down from the solution treatment temperature, they transform to low carbon martensite supersaturated with copper [1,3]. In the solution-annealed condition the ductility is low, therefore the formability is limited. After the solution heat treatment it can be hardened through the aging treatment of 1 to 4 h at 480 to 620°C (900 to 1150°F). The highest strength is obtained by aging at 480°C for 1h. In this condition copper particles are coherent with the martensitic matrix. The increase of aging temperature from 495 to 600°C leads to overaging, lowering the tensile strength but also enhancing the ductility as the copper particles growth and coarsen. The density of dislocations decreases and the amount of reverse austenite increases [1,3-8].

The weldability of 17-4PH is characterized in the literature as very good. It can be welded in solution-annealed conditions and overaged conditions [11-13]. It is not recommended to weld any material aged in 480°C/1h condition [12]. The previous studies focused on the influence of the post welding heat treatment (PWHT) on microstructure and mechanical properties [2,6,14]. PWHT provides similar properties of the fusion zone and the heat affected zone (HAZ) similar to the parent material [16]. Ziewiec investigated the cause of the microcracking in HAZ of fillet

[1] RZESZOW UNIVERSITY OF TECHNOLOGY, FACULTY OF MECHANICAL ENGINEERING AND AERONAUTICS, 12 POWSTAŃCÓW WARSZAWY AV., 35-959 RZESZÓW, POLAND
[2] PRATT & WHITNEY RZESZÓW, RZESZÓW, POLAND

* Corresponding author: agnieszka.nalborczyk@prattwhitney.com

weld joints. The reason for the development of cracks was steel embrittlement in the presence of liquid phase. This study points out that a good protection from oxidation is necessary as it reduces deformation and stress shrinkage [15]. Wanjara conducted research on electron beam welding of 17-4PH. This study examined the influence of various joining parameters on the without highlighting joint microstructure and mechanical properties. The solidification cracking was observed in the welded joint along the centre line. The decrease in the tendency of solidification cracking was obtained by the reduction of welding speed [16]. Laser and hybrid laser welding were also investigated. 17-4PH steel is susceptible to solidification cracking and formation of pores. Solidification cracking can by reduced by preheating and proper welding parameters. Main advantages of electron beam welding and laser beam welding are the possibility to achieve deep penetration, narrow weld and HAZ [4,12,17].

The main task of this research was to study the influence of TIG welding parameters of 17-4PH stainless steel on the microstructure of the welded joint. The research was focused on the impact of welding speed on the microstructure. The key idea was to determine optimal parameters of welding. The welded joints were made on flat samples. This research helps to verify whether any parameter changes influence the microstructure of 17-4PH stainless steel.

2. Materials and experimental methods

17-4PH stainless steel sheets with a thickness of 2 mm were used. The chemical composition of base metal is shown in TABLE 1.

TABLE 1

Chemical composition of 17-4PH stainless steel (wt %)

Percent by weight	Element									
	C	Mn	Si	P	S	Cr	Ni	Nb	Cu	Mo
Min	—	—	—	—	—	15,00	3,00	5xC	3,00	—
Max	0,07	1,00	1,00	0,040	0,030	17,00	5,00	0,45	5,00	0,50

Before welding the samples edges were grinded and then cleaned with isopropyl alcohol. Two samples of square groove weld were taken for research. The process of TIG welding was performed using a Fronius Magic Wave 4000 welding source and ABB IRB2600ID welding robot. The shielding gas was argon to prevent weld oxidation. The purity of the shielding gas was 99.9%. The welding parameters used for the welded joints are shown in TABLE 2. A fixture with cooper clamping was used from the root of the weld in order to absorb the heat. X-ray and fluorescent penetrant inspections were carried out after welding in order to check the internal discontinuity.

After welding, the samples were cut and subjected to heat treatment in protective atmosphere. First, test pieces were solution heat treated at 1040±10°C. Then ageing was carried out at 550±10°C for 4 h.

TABLE 2

Welding parameters

Parameters	Sample 1	Sample 2
Electrode diameter [mm]	3.2	3.2
Welding Speed [mm/s]	2.0	3.0
Main current [A]	125	125
Reduced Current [A]	100	100
Frequency [Hz]	7	7
Voltage [V]	8.5	8.6
Argon flow face of weld [L/min]	5	5
Argon flow root of weld [L/min]	6	6

Metallographic specimens for microscope analysis and hardness measurement were taken from the weld joints after the welding process and after the heat treatment. Metallographic cross section of the welded joints was prepared by grinding and polishing with the use of 1 μm diamond paste. The samples were analysed using Nikon Epiphot 300 light microscope and Hitachi S3400N (SEM) scanning electron microscope. The microstructure of the weld and heat affected zone was studied. The microhardness was measured using a 500 g load (Vickers microhardness), dwell time was 10 s. Measurements were performed on cross section of the weld joint 0.5 mm from the sheet edge using Innovatest machine. The spacing between indentations in the specimens after welding was 0.3 mm and in the welded joints after heat treatment was 0.4 mm. In order to determine the content of austenite after heat treatment, diffractometric tests were performed using ProtoiXRD. Test specimens were prepared in accordance with ASTM E3-11 and ASTM E975-13. $Cr_{K\alpha}$ radiation was used to determine the percentage of austenite V_γ. The test area was about 100-150 mm^2 and the depth up to 10-12 μm. Filtered chromium lamp (CrKα, $\lambda = 0.2293$ nm), with a voltage of 40 kV, current – 30 mA, range $2\theta = 10\text{-}80°$ was used. In order to determine the retained austenite on the diffractometric curve, two peaks from martensite 200_α and 211_α and two peaks from austenite 200_γ, 220_γ were analysed.

3. Results and discussion

3.1. Weld appearance and size

The visual inspection performed for both welded joints did not reveal any non-conformity such as the lack of penetration, undercut, underfill, or concavity. The fluorescent penetrant inspection and X-ray inspection did not detect any surface defects, porosity, voids or cracks in the welded joints.

The weld joints were made using different parameters, but the current value was the same for both the weld joints. Lower welding speed, thus higher heat input was applied to the weld joint of the first piece, resulting in a greater width of both face and root of the weld (TABLE 3). Hardness measurements show that the width of the HAZ is about 8.5 and 7 mm for Samples 1 and 2, respectively. The values for the weld face and the heat affected zone width are similar.

TABLE 3

Size of the face and root of weld

Sample	Width of weld face, mm	Width of weld root, mm
1	9.14	5.52
2	6.35	2.82

3.2. Fusion zone microstructure and hardness

In as-welded condition a weld joint consists of a weld, fusion zone (FZ), partly melted zone (PMZ) and heat affected zone (HAZ) (Fig. 1, 3). The fusion zone contains martensitic matrix with fine δ-ferrite located in the interdendritic regions (Fig. 5). The microstructure of as-welded condition shows a dendritic structure. The temperature for the transformation of austenite to martensite is 130 and 30°C [1]. The martensitic transformation

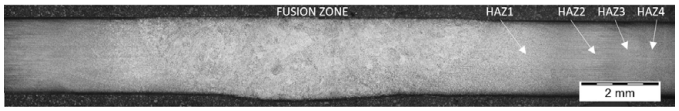

Fig. 1. Microstructure of cross-section of the welded joint 1

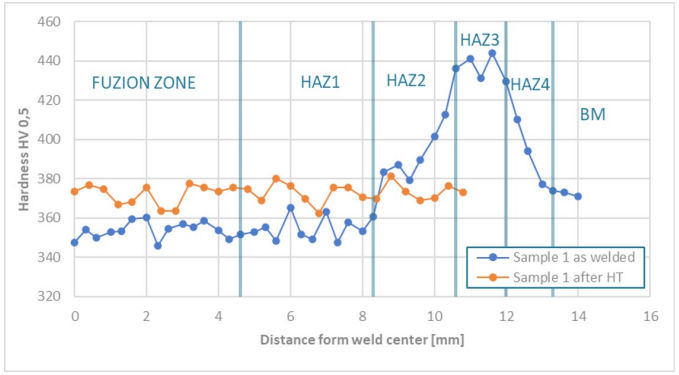

Fig. 2. Microhardness profile of the welded joint 1

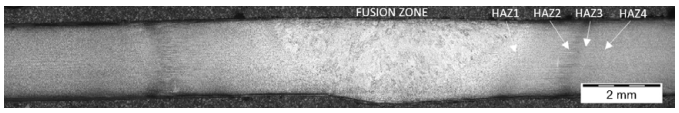

Fig. 3. Microstructure of cross-section of the welded joint 2

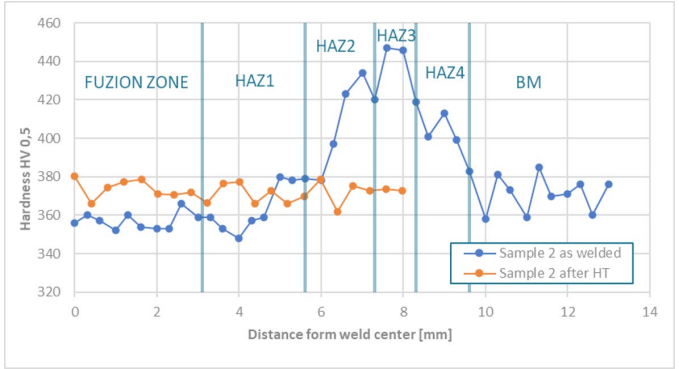

Fig. 4. Microhardness profile of the welded joint 2

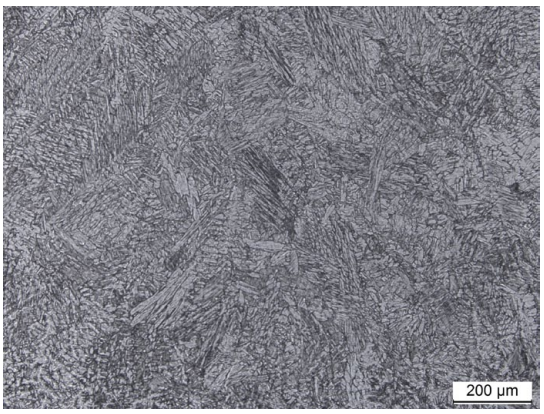

Fig. 5. Fusion weld micostructure of the welded joint 2 – marensite matrix with δ-ferrite at grain bouderies

finishes at the room temperature, so a minor quantity of retained austenite may be present in the microstructure [1,16].

Fig. 6 shows columnar grain growth from PMZ to the centre of the weld. A change in the direction of dendrite growth was observed in the centre of the weld line in Sample 2 (Fig. 6d). The microhardness profile is presented in Fig. 2 and 4. The hardness of the fusion zone of Sample 1 measured at 348-359 HV is a bit lower than the hardness of Sample 2 – 353-366 HV. Higher heat input was applied to Sample 1 which could result in grain growth of the fusion zone.

3.3. Heat affected zone microstrcture and hardness

The microstructure in HAZ depends on heating and cooling conditions during a welding process. Based on microstructure observations and microhardness measurements, 4 regions (HAZ1, HAZ2, HAZ3, HAZ4) can be distinguished in the heat affected zone. The highest temperature occurs near the fusion line and decreases with the distance from the weld line. Coarse delta ferrite is present in the partly melted zone. Delta ferrite is formed along the prior austenite grain boundaries at HAZ1 perpendicular to FZ (Fig. 7, 8a,b). On the root side the bands of δ-ferrite are longer than from the side of the face of weld. The solidification of 17-4 PH is primary ferrite mode [6]. The transformations during the cooling phase can be determined as follows:

$$L \rightarrow \delta\text{-ferrite} \rightarrow \text{austenite} + \delta\ \text{ferrite} \rightarrow \text{martensite} + \\ + \delta\text{-ferrite}\ [6]$$

Rapid cooling adjacent to weld fusion zone suppresses diffusion transformation of δ-ferrite to austenite. The welding fixture from the root side is made of cooper. It ensures faster cooling rate, which can explain the increase in the quantity of δ-ferrite. HAZ1 is a two-phase region consisting of δ-ferrite and retransferred martensite. The grain size exhibit prior austenite grain is visually larger near weld line. As the distance from the fusion line increases, the grain size decreases. In this area the carbides were dissolved and the hardness within the first region is similar to the fusion zone.

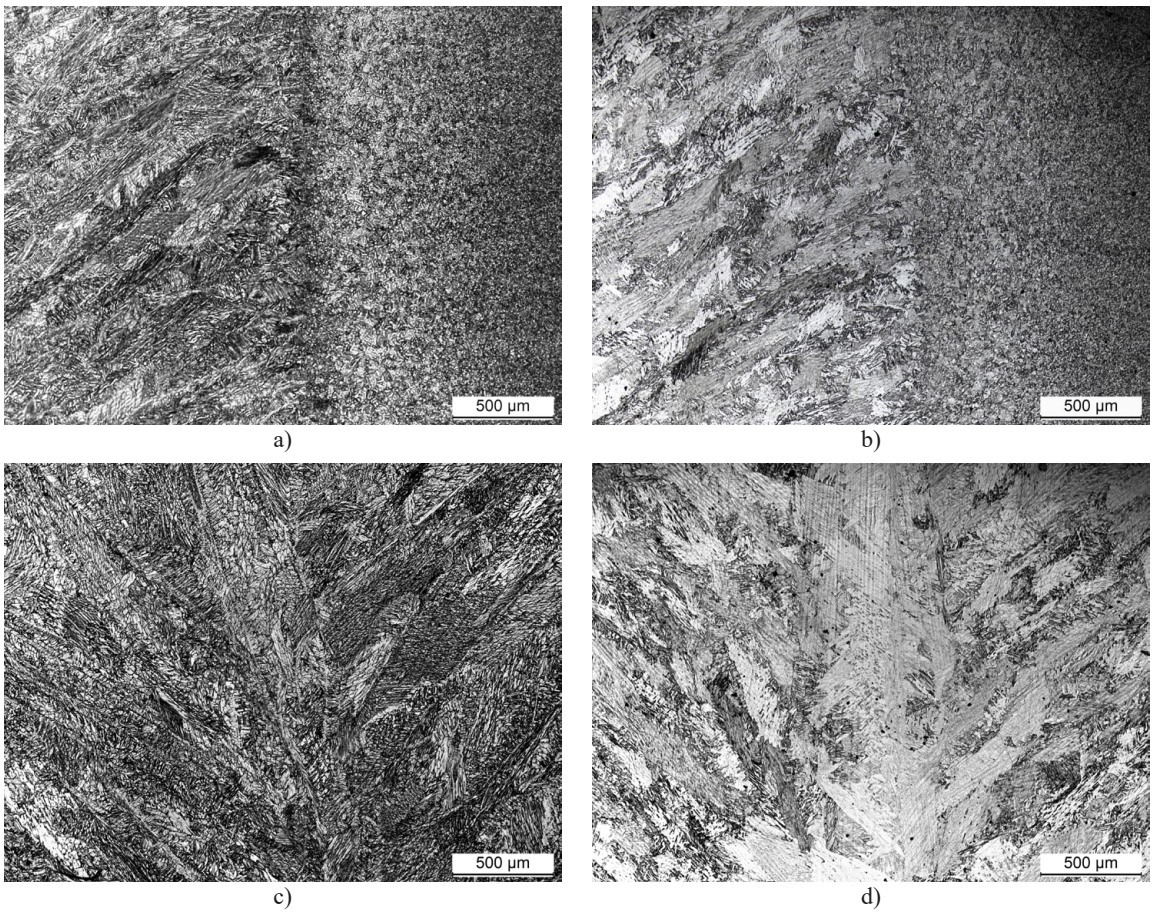

a) b) c) d)

Fig. 6. Microstructure of longitudinal section of a), c) the welded joint 1, and b), d) the welded joint 2

During tge transition from HAZ1 to HAZ2 an increase of hardness (to 380 HV) and the microstructure change form light to the dark etched region were observed. This region was experiencing a lower temperature (above 704°C). During the cooling phase the transformation of austenite into martensite occurred and new untempered martensite was formed. The grain size is smaller in comparison to the HAZ1. Undissolved NbC carbides remain at the grain boundaries (Fig. 9). According to Wanjara, precipitation of chromium carbides could start in this region at the temperature of 700-900°C [16].

Microstructure observations indicate that the area of HAZ3 was heated up to Ac_1 which acc. to the literature is about 627°C [16]. In this area, the newly formed martensite can coexist with the tempered martensite. The microstructure changes from dark to light etched region similar to the base material. The peak of hardness up to 447 HV is observed in this region. It is caused by the aging of martensite through the precipitation of Cu-rich particles. The standard aging temperature range is 480-620ºC [1]. The hardness obtained within HAZ3 is similar to the effect of aging at 480°C for 1 h leading to the highest strength of 17-4PH SS. In the next area the hardness starts to decrease to reach the value of the base material. The increased hardness compared to the base material indicates that the ageing process has started. This region was heated up below 620°C. Under the light microscope, no differences were observed between the microstructure of HAZ4 and the parent material.

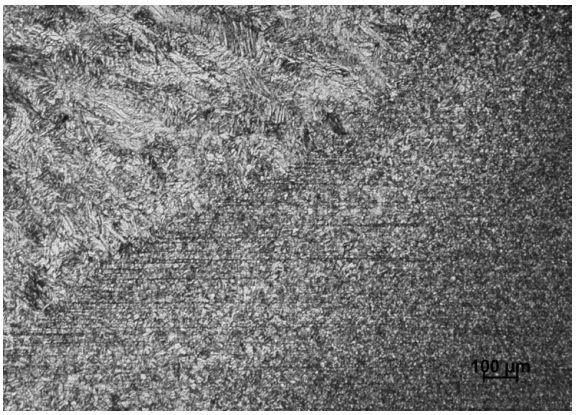

Fig. 7. Microstructure of the fusion weld and heat affected zone

3.4. Weld joint microstructure after precipitation hardening treatment

Solution and aging heat treatment affected the microstructure and hardness of the weld joint. The hardness is almost the same for Sample 1 and 2 within the range of 360-380 HV in the entire weld joint. The grain size differences in the heat affected zone remains visible, but there is no difference in the etching shade. The observation of the microstructure shows that the amount of δ-ferrite present at the fusion line in the as-welded condition is significantly reduced after the heat treatment. It shows

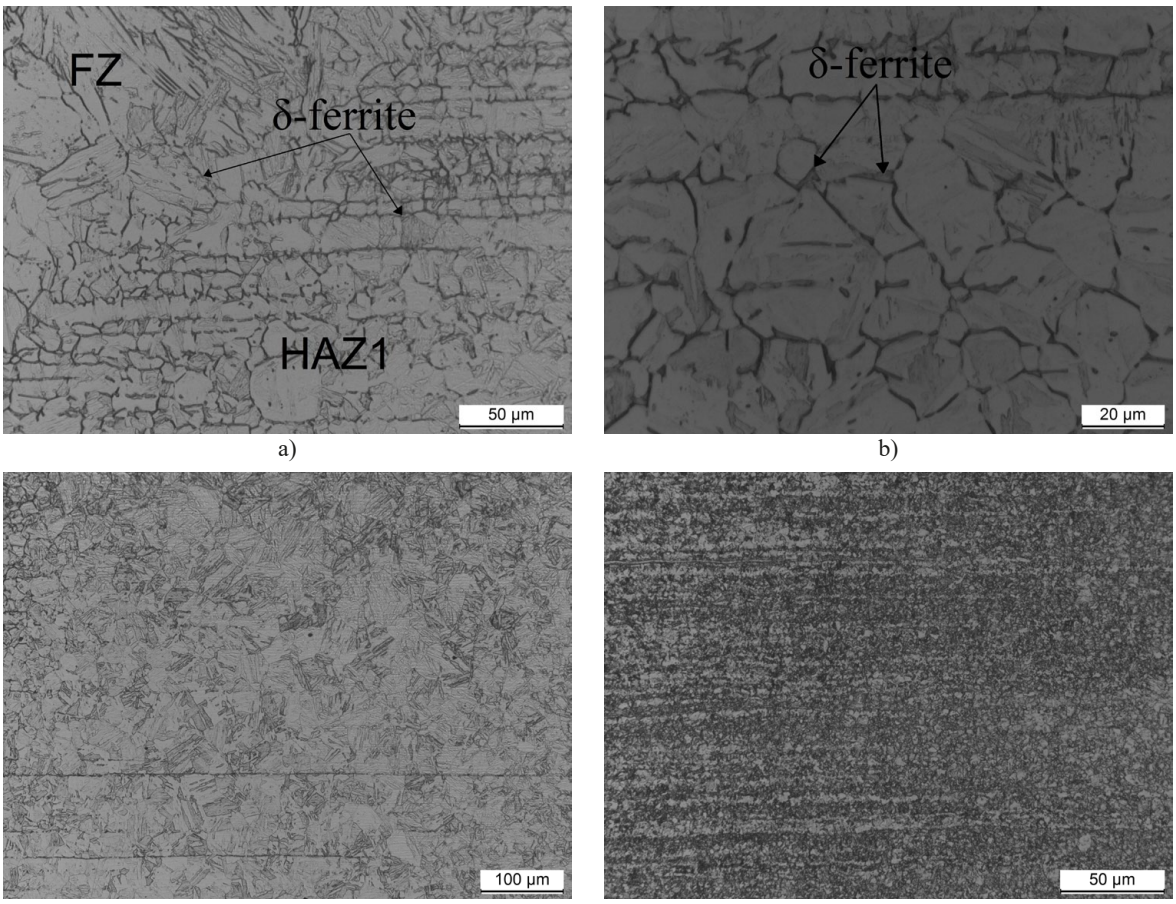

Fig. 8. Microstructure of a) partly melted zone and δ-ferrite, b) δ-ferrite, c) large grain of HAZ1, d) dark etched region of HAZ2

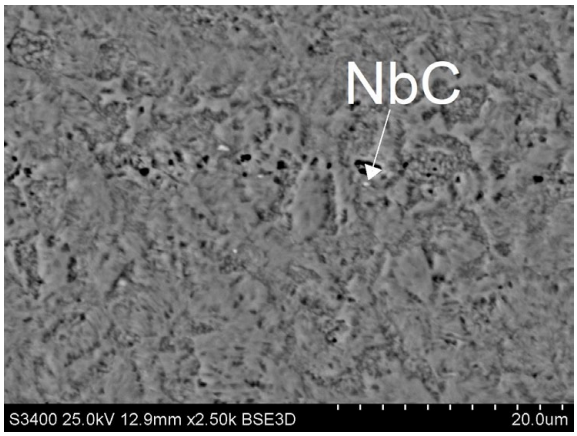

a)

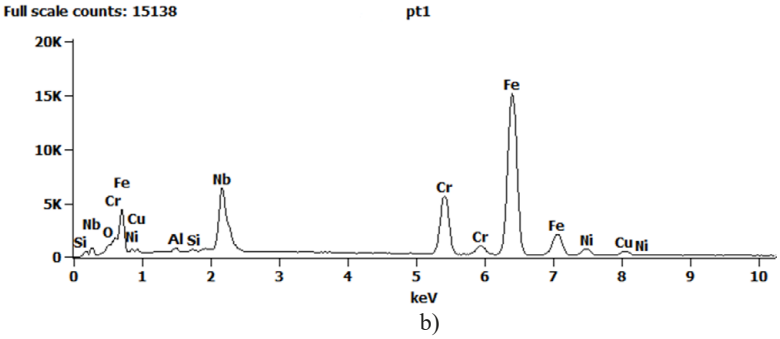

b)

Weight %

	O-K	Al-K	Si-K	Cr-K	Fe-K	Ni-K	Cu-K	Nb-L
pt1	0.0	0.5	0.3	14.5	59.4	3.2	2.3	19.8

Weight % Error (+/- 1 Sigma)

	O-K	Al-K	Si-K	Cr-K	Fe-K	Ni-K	Cu-K	Nb-L
pt1	±0.0	±0.0	±0.0	±0.1	±0.2	±0.1	±0.1	±0.2

Atom %

	O-K	Al-K	Si-K	Cr-K	Fe-K	Ni-K	Cu-K	Nb-L
pt1	0.0	1.1	0.6	16.7	63.5	3.2	2.2	12.7

Atom % Error (+/- 1 Sigma)

	O-K	Al-K	Si-K	Cr-K	Fe-K	Ni-K	Cu-K	Nb-L
pt1	±0.0	±0.1	±0.1	±0.1	±0.2	±0.1	±0.1	±0.1

c)

Fig. 9. SEM image of the heat affected HAZ2

that the transformation of δ-ferrite into austenite took place during the cooling process. The fine network of δ-ferrite is visible at the grain boundaries of the tempered martensitic matrix. X-ray diffraction detected stable austinite in the weld joints. 3.19% and 3.42% for Sample 1 and 2, respectively. Retained austenite remains in the microstructure because the M_f temperature is close to the ambient temperature. Burja shows that with the higher ageing temperatures the portion of reversed austenite increases and the analysis performed by ThermoCalc shows that the quantity of austenite after ageing at 550°C could reach 5.8%.

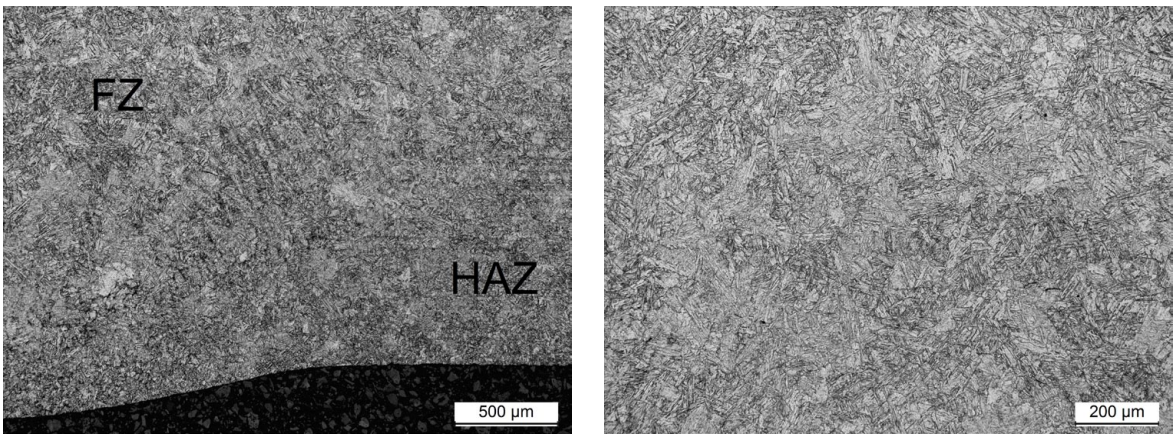

a) b)

Fig. 10. Microstructure of weld joint after heat treatment a) weld and HAZ b) fusion zone

The mechanism of austenite formation during aging has not been thoroughly investigated for 17-4PH steel. It is supposed that austenite is formed at the local segregation of austenite stabilizing elements (Cu, Ni), which cause a decrease of the austenitic transformation temperature [7,18]. The solution and aging heat treatment homogenized to some extent the microstructure and hardness in the welded joints.

4. Conclusions

In this study the microstructure characteristic and hardness of 17-4 PH SS welded joints were investigated using robotic TIG and the following results were obtained:

- Conforming welded joints free from defects were obtained by robotic TIG welding.
- Heat input resulting from the parameters used affects the size of the weld and the HAZ. The width of the fusion zone and the HAZ increases with higher heat input. The nature of changes occurring in the heat affected zone in the microstructure is the same for both samples. However, the hardness of the fusion zone is a bit lower when a lower welding speed is used.
- Due to the differences of microstructure and hardness, the heat affected zone can be divided into 4 areas depending on it thermal history.
- The weld joint after solution and aging at 550°C contains about 3% austenite.

REFERENCES

[1] ASM Handbook, Volume 4D, Heat Treating of Irons and Steels, 2014 ASM International.

[2] A.K. Bhaduri, S. Sujith, G. Srinivasan, T P.S Gill, S.L. Mannan, Welding Journal **74** (5), 153-159 (1995).

[3] S.S.M. Tavares, Jurnal of Material Enginering and Performance **26** (6), 2512-2518 (2017).

[4] M.B. Balajaddeh, H. Naffakh-Moosavy, Optics & Laser Technology **119**, 1-12 (2019).

[5] C. Chen-Yuan, T. Yu-Chih, Materials Letters **237**, 228-231 (2019).

[6] A. Ziewiec, A. Zielińska-Lipiec, E. Tasak, Archives of Metallurgy and Materials **59** (3), 965-970 (2014).

[7] C.N. Hsiao, C.S. Chiou, J.R. Yang, Materials Chemistry and Physics **74**, 134-142 (2002).

[8] S.S.M. Tavares, F.J. da Silva, C. Scandian, G.F. da Silva, H.F.G. de Abreu, Corrosion Science **52** (11), 3835-3839 (2010)

[9] T. Trzepieciński, T. Pieja, T. Malinowski, R. Smuszc, M. Motyka, Journal of Materials Processing Tech. **252**, 192-200 (2018)

[10] J. Burja, B. Šuler, A. Nagode, Materialwissenschaft und Werkstofftechnik **50**, 405-411(2019)

[11] C.R. Das, H.C. Dey, G. Srinivasan, S.K. Albert, A.K. Bhaduri, A. Dasgupta, Science and Technology of Welding and Joining **11** (5), 502-508 (2006).

[12] W. Liu, J. Ma, M.M. Atabaki, R. Pillai, B. Kumar, U. Vasudevan, H. Sreshta, R. Kovacevic, Hybrid laser-arc Welding of 17-4PH Martensitic Stainless Steel. Lasers in Manufacturing and Materials Processing **2**, 74-90 (2015).

[13] ASM Handbook, Volume 6,Welding, Brazeing and Soldering 1993 ASM International

[14] K. Bhaduri, T.P.S. Gill, G. Srinivasan, S. Sujith, Science and Technology of Welding and Joining **4** (5), 295-301 (1999).

[15] A. Ziewiec, J. Czech, E. Tasak, Archives of Metallurgy and Materials **57** (4), 1055-1060 (2012).

[16] P. mayjara, M. Jahazi, Canadian Metallurgical Quarterly **47** (4), 413-435 (2008).

[17] J. Ma, M.A. Mehdi, L. Wei R. Pillai, B. Kumar, U. Vasudevan, R. Kovacevic, Optics & laser Technology **82**, 38-52 (2016).

[18] R. Bhambroo, S. Roychowdhury, K. Vivekanand, V.S. Raja, Materials Science & Engineering A **568**, 127-133 (2013).